J. Fluid Mech. (2014), *vol.* 751, *pp.* 406–431.
doi:10.1017/jfm.2014.281

Long-wave dynamics of an inextensible planar membrane in an electric field

Y.-N. Young[1,†], Shravan Veerapaneni[2] and Michael J. Miksis[3]

[1]Department of Mathematical Sciences and Center for Applied Mathematics and Statistics, New Jersey Institute of Technology, Newark, NJ 07102, USA

[2]Department of Mathematics, University of Michigan, Ann Arbor, MN 48109, USA

[3]Department of Engineering Sciences and Applied Mathematics, Northwestern University, Evanston, IL 60208, USA

(Received 11 November 2013; revised 18 March 2014; accepted 19 May 2014; first published online 20 June 2014)

In this paper the dynamics of an inextensible capacitive elastic membrane under an electric field is investigated in the long-wave (lubrication) leaky dielectric framework, where a sixth-order nonlinear differential equation with an integral constraint is derived. Steady equilibrium profiles for a non-conducting membrane in a direct current (DC) field are found to depend only on the membrane excess area and the volume under the membrane. Linear stability analysis on a tensionless flat membrane in a DC field gives the growth rate in terms of membrane conductance and electric properties in the bulk. Numerical simulations of a capacitive conducting membrane under an alternating current (AC) field elucidate how variation of the membrane tension correlates with the nonlinear membrane dynamics. Different membrane dynamics, such as undulation and flip-flop, are found at different electric field strength and membrane area. In particular a travelling wave on the membrane is found as a response to a periodic AC field in the perpendicular direction.

Key words: biological fluid dynamics, membranes, thin films

1. Introduction

The cellular membrane, comprising mainly two lipid leaflets, is essential to a wide range of cellular functions partly because the membrane regulates the transport of particles (such as ions and macromolecules) between interior and exterior cellular space. The cellular membrane possesses a capacitance and a conductance, and both weak (Antov *et al.* 2005) and strong electric fields are used to induce membrane deformation and poration for delivering drug and/or DNA into living cells (see Sadik *et al.* 2011 and references therein). External direct current (DC) and/or alternating current (AC) electric fields have also been used to destabilize planar lipid membranes for the formation of vesicles (liposomes, self-enclosing unilamellar membranes) in electroformation (Angelova & Dimitrov 1986; Angelava & Dimitrov 1987; Angelova *et al.* 1992; van Swaay & deMello 2013), where the interplay between external electric fields and the membrane forces (such as membrane tension and bending

† Email address for correspondence: yyoung@oak.njit.edu

forces) underlies the membrane instability. Experimental studies have revealed that AC electric fields can effectively unbind a stack of lipid bilayer membranes close to a substrate (Constantin *et al.* 2005; Lecuyer, Fragneto & Charitat 2006). It is further found that the AC electric fields with frequencies below 100 Hz are more effective in amplifying the fluctuations of a floating bilayer membrane (Lecuyer *et al.* 2006). For giant vesicles under an electric field, the electric pulse duration and the subsequent relaxation process are found to be essential to membrane deformation and poration (Riske & Dimova 2005; Bezlyepkina *et al.* 2009; McConnell, Miksis & Vlahovska 2013; Zhang *et al.* 2013).

The biological lipid membrane immersed in an ionic solution has been modelled as a thin film of non-Newtonian fluid (Maldarelli, Jain & Ivanov 1980; Maldarelli & Jain 1982). Theoretical studies on the stability of a planar membrane under electric fields show that both membrane thickness fluctuations (Weaver & Chizmadzhev 1996) and bending modes (Sens & Isambert 2002; Lacoste, Lagomarsino & Joanny 2007; Schwalbe, Vlahovska & Miksis 2011) may contribute to destabilization. Sens & Isambert (2002) found negative membrane tension and the ion currents in the diffuse layers near the membrane give rise to undulations of an unsupported planar membrane under electric fields. Once the electric field is above a threshold, the planar membrane becomes unstable and the undulation can be amplified. The linear response regime of a planar membrane in electrolyte under a DC field has been investigated (Lacoste *et al.* 2007, 2009; Ziebert, Bazant & Lacoste 2010; Ziebert & Lacoste 2010, 2011). Having incorporated the capacitive effects of both the membrane and the Debye layers, the electrostatic corrections to the elastic moduli due to finite membrane thickness are computed and the resultant linear growth rate is obtained.

Membrane conductance and mismatch in dielectric properties of surrounding fluids are also essential to the linear instability of a planar lipid bilayer membrane in both DC (Seiwert, Miksis & Vlahovska 2012) and AC (Seiwert & Vlahovska 2013) electric fields. Without membrane conductance it is found that mismatch in the bulk conductivities gives rise to a transient instability in a DC field (Schwalbe *et al.* 2011). With membrane conductance, the capacitive membrane can be linearly unstable (Seiwert *et al.* 2012). In an AC electric field a purely capacitive membrane can be rendered unstable at low field frequencies, while at high frequencies even a conducting membrane can become stable (Seiwert & Vlahovska 2013).

Long-wave (lubrication) models of the electrohydrodynamics of an interface between two leaky dielectric fluids under DC or AC (see Roberts & Kumar 2009, 2010) fields have uncovered both the linear instability and weakly nonlinear dynamics related to pillar formation that are consistent with experiments (Schaffer *et al.* 2000; Pease & Russel 2002; Thaokar & Kumaran 2005; Wu & Russel 2009). The lubrication theory has also been successfully applied to understand the elastohydrodynamics of an elastic sheet lubricated by a thin layer of fluid (Hosoi & Mahadevan 2004). In that analysis the bending force is dominant over the tension, and the elastic sheet area may vary due to the dynamics. The balance between bending force and the van der Waals forces was found essential to the observed bursting in the elastic sheet with a constant flux in the lubricating layer. More recently Blount, Miksis & Davis (2012) developed a lubrication model to study flow beneath a semipermeable inextensible membrane and obtained equilibrium solutions and bifurcation structure as a function of drying parameters.

In this work, we apply the long-wave analysis to two layers of leaky dielectric fluid separated by an elastic inextensible membrane which is a sharp-interface model for the lipid bilayer membrane. The main components of the sharp-interface

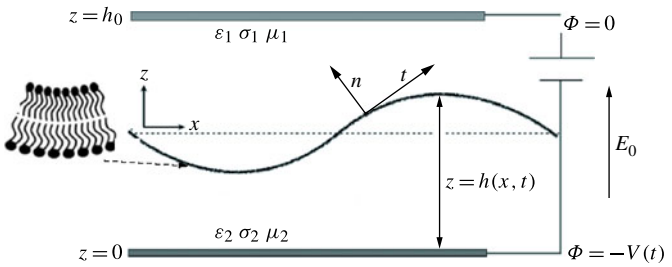

FIGURE 1. A planar lipid bilayer membrane (at height $z = h(x, t)$) separates two leaky dielectric fluids. The electric potential Φ is fixed on the top electrode ($\Phi = 0$) and bottom electrode ($\Phi = -V(t)$). Here $\boldsymbol{n}$ is the outward unit normal on the membrane, and $\boldsymbol{t}$ is the unit tangent. The bulk fluid is characterized by permittivity (ε), conductivity (σ) and viscosity (μ).

approximation of the lipid bilayer membrane are its elastic properties, inextensibility, capacitance and conductance. The lipid bilayer membrane is inextensible because both the area per lipid and the total lipid number are conserved in each leaflet. In this work we use membrane forces derived from the Helfrich membrane energy $\mathscr{F} = \int_\Omega ((\kappa/2)H^2 + \Sigma)\,\mathrm{d}\Omega$, where Ω is the membrane surface, κ is the bending modulus, and H is the mean curvature. The membrane tension Σ is a Lagrange multiplier to be determined from the constant surface area constraint (Seifert 1995). The inextensible elastic membrane also acts as a (leaky) capacitor where the trans-membrane potential varies due to the currents on and across the two leaflets. In biological cells the trans-membrane currents may be due to pores and ion channels. The currents on the membrane are the ohmic currents from the bulk to the membrane in the leaky dielectric model.

The general goal of this work is to elucidate the nonlinear dynamics of a capacitive membrane under an electric field. Specifically, we will consider the dynamics of a planar membrane separated by two leaky dielectric fluids and bounded by two planar electrodes (see figure 1). This simple geometry is canonical and allows a detailed examination of the effect of the electric field on the nonlinear membrane dynamics. As noted above, planar geometries have been studied by several authors in the linearized case to get a better understanding of membrane dynamics. In addition the geometry is pertinent to electroformation experiments where planar membranes are driven unstable by an electric field across an elongated microfluidic channel (Angelova & Dimitrov 1986; Angelava & Dimitrov 1987; Angelova *et al.* 1992; van Swaay & deMello 2013).

This paper is organized as follows. The problem description is given at the beginning of § 2, followed by § 2.1 where we formulate the long-wave dynamics of an elastic, inextensible membrane separating two leaky dielectric fluids. The equilibrium profile for a non-conducting membrane in a DC field is derived in § 2.2, and the linear stability for a flat tension membrane in a DC field is analysed in § 2.3. The numerical implementation of a semi-implicit scheme for solving the governing long-wave equations is given in § 2.4. In a DC field the displacement current is negligible and our numerical simulations show that the membrane dynamics (with or without membrane conductance) is always towards the steady equilibrium that is similar to those described in § 2.2. Therefore in § 3 we focus on the dynamics of a conducting membrane in an AC field. We first examine the linear stability of a tensionless flat membrane in an AC field in § 3.1. In the rest of § 3 we study how

the membrane instability and its nonlinear dynamics depend on the membrane tension and the correlation with induced surface charge distribution. In § 3.4 we present a novel 'alternating wave' with large membrane excess length under strong AC fields. We summarize our findings and provide a discussion on the implications of the results in § 4.

2. Problem formulation

We consider two layers of leaky dielectric fluid under an imposed electric field $E_0\hat{z}$. The two fluids are separated by an inextensible elastic planar membrane (at $z=h(x,t)$) formed by a charge-free lipid bilayer with dielectric constant ε_m and conductivity σ_m. The bilayer thickness $d\sim 5$ nm, which is small enough for us to treat the membrane as a two-dimensional interface with effective capacitance $C_m=\varepsilon_m/d$ and conductance $G_m=\sigma_m/d$. As shown in figure 1, each layer of fluid is specified by its permittivity (ε), conductivity (σ) and viscosity (μ), with the subscripts in figure 1 denoting either top ('1') or bottom ('2') fluid layer. The electric field is irrotational, $\boldsymbol{E}_j=-\boldsymbol{\nabla}\Phi_j$. In the leaky dielectric framework, the bulk charge is assumed to be zero as the bulk charge relaxes over a charging time $t_{c,j}=\varepsilon_j/\sigma_j\ll 1$. Therefore the electric potential Φ satisfies the Laplace equation

$$\nabla^2\Phi_j=0,\quad j=1,2. \tag{2.1}$$

Within each layer the two-dimensional fluid velocity $\boldsymbol{u}_j=(u_j,\,w_j)$ satisfies the incompressible Navier–Stokes equations

$$\rho_j\left(\frac{\partial \boldsymbol{u}_j}{\partial t}+\boldsymbol{u}_j\cdot\boldsymbol{\nabla}\boldsymbol{u}_j\right)=-\boldsymbol{\nabla}p_j+\mu_j\nabla^2\boldsymbol{u}_j, \tag{2.2}$$

$$\boldsymbol{\nabla}\cdot\boldsymbol{u}_j=0, \tag{2.3}$$

where $j=1$ or $j=2$ for the top or bottom fluid. Here p_j is pressure, and ρ_j is the fluid density which we assume to be the same for both layers.

To complete the formulation of the problem, boundary conditions for the electric potential are needed across the membrane. As noted earlier, the membrane is assumed to be a capacitor which can accumulate surface charge on both of its sides. Following Seiwert *et al.* (2012) and Seiwert & Vlahovska (2013), the trans-membrane potential $V_m=\Phi_2-\Phi_1$ on $z=h(x,t)$ can be determined from the conservation of normal current. The result is

$$C_m\left(\frac{\partial V_m}{\partial t}+\boldsymbol{u}\cdot\boldsymbol{\nabla}_s V_m\right)+G_m V_m=\sigma_i E_i+\varepsilon_i\left(\frac{\partial E_i}{\partial t}+\boldsymbol{u}\cdot\boldsymbol{\nabla}_s E_i\right) \tag{2.4}$$

for $i=1,2$ along $z=h(x,t)$. Here we define the normal electric field as $E_i\equiv\boldsymbol{n}\cdot\boldsymbol{E}_i$ and $\boldsymbol{\nabla}_s=(\boldsymbol{I}-\boldsymbol{nn})\boldsymbol{\nabla}$ is the surface gradient. The membrane capacitance is approximately $C_m\approx 0.01$ F m^{-2} and the membrane conductance varies over the range $G_m\approx 10^{-3}-10^{6}$ S m^{-2}. Note that the total surface charge can now be defined as $q=\varepsilon_1E_1-\varepsilon_2E_2$. For completeness, details of the derivation of this boundary condition can be found in appendix A.

2.1. *Long-wave formulation*

In the long-wave formulation, the aspect ratio (ϵ) of the height (h_0) to the characteristic horizontal length (l) is assumed to be small: $\epsilon = h_0/l \ll 1$. Similar to the scaling in Hosoi & Mahadevan (2004), we non-dimensionalize equations (2.1)–(2.4) by the characteristic length and velocity (h_0/ϵ, h_0) and (U_0, ϵU_0) in the (x, z) directions, respectively. The pressure is scaled by $\mu_2 U_0/\epsilon h_0$, time by $h_0/\epsilon U_0$, and the electric potential by $E_0 h_0$. The dimensionless variables (with bars) are

$$\left.\begin{gathered}\bar{z} = \frac{z}{h_0}, \quad \bar{x} = \frac{x}{h_0/\epsilon}, \quad \bar{u} = \frac{u}{U_0}, \quad \bar{w} = \frac{w}{\epsilon U_0}, \quad \bar{p} = \frac{p}{\mu_2 U_0/\epsilon h_0}, \\ \bar{t} = \frac{t}{h_0/\epsilon U_0}, \quad \text{and} \quad \bar{V}_m = \frac{V_m}{E_0 h_0}.\end{gathered}\right\} \tag{2.5}$$

The dimensionless equations are (after dropping bars)

$$\epsilon Re_i \left(\partial_t u_i + u_i \partial_x u_i + w_i \partial_z u_i\right) = -\frac{\mu_2}{\mu_i}\partial_x p_i + \partial_z^2 u_i + \epsilon^2 \partial_x^2 u_i, \tag{2.6}$$

$$\epsilon^3 Re_i \left(\partial_t w_i + u_i \partial_x w_i + w_i \partial_z w_i\right) = -\frac{\mu_2}{\mu_i}\partial_z p_i + \epsilon^2 \left(\partial_z^2 w_i + \epsilon^2 \partial_x^2 w_i\right), \tag{2.7}$$

$$\partial_x u_i + \partial_z w_i = 0, \tag{2.8}$$

$$\nabla^2 \Phi_i = \partial_{zz}^2 \Phi_i + \epsilon^2 \partial_{xx}^2 \Phi_i = 0, \tag{2.9}$$

$$c_m \left(\frac{\partial V_m}{\partial t} + u\frac{\partial V_m}{\partial x}\right) + g_m V_m = E_1 + \alpha \left(\frac{\partial E_1}{\partial t} + u\frac{\partial E_1}{\partial x}\right), \tag{2.10}$$

$$E_1 + \alpha \left(\frac{\partial E_1}{\partial t} + u\frac{\partial E_1}{\partial x}\right) = \frac{1}{\sigma_r}E_2 + \frac{\alpha}{\varepsilon_r}\left(\frac{\partial E_2}{\partial t} + u\frac{\partial E_2}{\partial x}\right). \tag{2.11}$$

The dimensionless parameters are

$$Re_i \equiv \frac{U_0 h_0}{\mu_i/\rho_i}, \quad \alpha = \frac{\varepsilon_1 U_0}{h_0 \sigma_1}\epsilon, \quad c_m = \frac{C_m U_0}{\sigma_1}\epsilon, \quad \text{and} \quad g_m = \frac{G_m h_0}{\sigma_1}. \tag{2.12}$$

There are several time scales involved in this system: the capacitive membrane charges on a time scale (Seiwert & Vlahovska 2013) $t_m = (h_0 C_m/\sigma_1)[(1+\sigma_r)/(1+g_m(1+\sigma_r))]$, the balance between viscous stress and the electric shear traction gives $t_{EHD,j} = \mu_j/\varepsilon_j E_0^2$, while bending resistance to changes in membrane curvature gives another time scale $t_{\kappa,j} = \mu_j/\kappa Q^3$ for a membrane undulation with wavenumber Q. Typical values are for the conductivity $\sigma \approx 10^{-6}$–10^{-3} S m^{-1}, $\varepsilon \approx 10^{-10}$ F m^{-1}, $\kappa \approx 10^{-19}$ J, $h_0 \approx 100$ μm to several mm, $\mu \approx 10^{-3}$ Pa s, $E_0 \approx$ 1–6 kV m^{-1}. We choose $U_0 = \sigma_1/C_m\epsilon$ such that $c_m = 1$, and typically $U_0 \approx O(1)$ due to the small conductivity and large membrane capacitance.

At the bottom wall $u_2(0) = w_2(0) = 0$ and $\Phi_2(0) = -v(t)$, while at the top wall $u_1(1) = w_1(1) = 0$ and $\Phi_1(1) = 0$. On the elastic membrane $z = h(x, t)$, the kinematic boundary condition (or no-slip boundary condition) gives

$$w_1(x, h(x,t)) = w_2(x, h(x,t)) = \partial_t h + u_1|_{z=h}\partial_x h = \partial_t h + u_2|_{z=h}\partial_x h. \tag{2.13}$$

The stress balance on the elastic membrane gives

$$(-p_1 + p_2)\,\boldsymbol{n} + [\![\boldsymbol{T}^{hd} + \boldsymbol{T}^{el}]\!] \cdot \boldsymbol{n} = \boldsymbol{f}^m, \tag{2.14}$$

where $[\![\cdot]\!]$ denotes the difference between top and bottom layers. Here $(\boldsymbol{T}^{hd})_{ij} \equiv \mu(\partial_i v_j + \partial_j v_i)$ is the ijth component of the viscous stress tensor, and $(\boldsymbol{T}^{el})_{ij} \equiv \varepsilon(\boldsymbol{E}_i\boldsymbol{E}_j - \boldsymbol{E}^2\delta_{ij}/2)$ is the ijth component of the Maxwell electric stress. The membrane force $\boldsymbol{f}^m = \kappa[4H^3 - 4HH_G + 2\nabla_s^2 H]\boldsymbol{n} - 2\Sigma H\boldsymbol{n} + \nabla_s\Sigma$, where κ the membrane bending rigidity, H the membrane mean curvature, H_G is the Gaussian curvature, and Σ the membrane surface tension to be determined from the membrane incompressibility condition. For the planar geometry in the long-wave limit, the Gaussian curvature is zero and we ignore the high-order curvature term. Hence $\boldsymbol{f}^m = -(-2\kappa\nabla_s^2 H + 2\Sigma H)\boldsymbol{n} + \nabla_s\Sigma$.

Following the procedures in the lubrication analysis for a porous inextensible elastic membrane (Blount *et al.* 2012), the dependent variables (u, w, p) are expanded in ϵ and (Φ, Σ) in ϵ^2. At leading order the membrane outward normal $\boldsymbol{n} = (-\epsilon\partial_x h, 1)/\sqrt{1+\epsilon^2\partial_x h^2} \sim (-\epsilon\partial_x h, 1)$, the membrane tangent $\boldsymbol{t} = (1, \epsilon\partial_x h)/\sqrt{1+\epsilon^2\partial_x h^2}$ $\sim (1, \epsilon\partial_x h)$, and the membrane curvature $H \equiv \epsilon^2 h_{xx}/(1+\epsilon^2\partial_x h^2)^{3/2} \sim \epsilon^2 h_{xx}$. The leading-order electric potential in the bulk satisfies the equation $\partial_{xx}^2\Phi = 0$ and can be computed as $\Phi_1 = E_1(x,t)(z-1)$ and $\Phi_2 = E_2(x,t)z - v(t)$ with $v(t) = V(t)/V_0$.

The normal stress balance at $z = h$ gives a relation between p_1 and p_2, and the tangential stress balance at $z = h$ gives a relation between the Marangoni stress and the viscous shear stress. At leading order, the horizontal velocity field can be written as $u_i = (\mu_2/\mu_i)(\partial_x p_i/2)z^2 + a_i z + b_i$, where a_i and b_i are to be determined by the velocity boundary conditions (Oron, Davis & Bankoff 1997):

$$a_1 + b_1 = -\frac{1}{2\mu_r}(p_2 + g + \beta_1)_x \equiv D', \tag{2.15}$$

$$ha_1 + b_1 - ha_2 = \frac{h^2}{2}\left[p_2\left(1 - \frac{1}{\mu_r}\right) - \frac{g+\beta_1}{\mu_r}\right]_x \equiv E', \tag{2.16}$$

$$\mu_r a_1 - a_2 = h(-g-\beta_1)_x - \frac{\bar{C}}{2}\partial_x\Sigma_1 - \beta_2 \equiv F', \tag{2.17}$$

with $\beta_2 \equiv \beta\left[\varepsilon_r\left(E_1E_{1x}(h-1) - E_1^2 h_x\right) - (E_{2x}h - E_2h_x)E_2\right]$, $g \equiv \bar{C}\Sigma_0\partial_x^2 h - \varkappa\partial_x^4 h$, and $\beta_1 \equiv (\beta/2)\left(\varepsilon_r E_1^2 - E_2^2\right)$. Equation (2.15) is from $u_1 = 0$ at $z = 1$, equation (2.16) corresponds to $u_1 = u_2$ at $z = h$, and (2.17) is from the shear stress balance at $z = h$. In addition, $b_2 = 0$ because $u_2 = 0$ at $z = 0$.

The dimensionless parameters in the above equations are defined as

$$\beta \equiv \frac{\varepsilon_2 E_0^2 h_0\epsilon}{\mu_2 U_0} = \frac{\varepsilon_2 E_0^2 h_0 C_m\epsilon^2}{\mu_2\sigma_1}, \quad \varkappa \equiv \frac{2\kappa\epsilon^5}{\mu_2 U_0 h_0^2} = \frac{2\kappa C_m\epsilon^6}{\mu_2\sigma_1 h_0^2}, \quad \bar{C} \equiv \frac{2\gamma_0\epsilon^3}{\mu_2 U_0} = \frac{2\gamma_0 C_m\epsilon^4}{\mu_2\sigma_1}, \tag{2.18}$$

where γ_0 is a scaling factor for membrane tension, the viscosity ratio $\mu_r = \mu_1/\mu_2$, conductivity ratio $\sigma_r = \sigma_1/\sigma_2$, and permittivity ratio $\varepsilon_r = \varepsilon_1/\varepsilon_2$. The solution (a_1, b_1, a_2) is computed as

$$a_1 = \frac{D' - E' + F'h}{1 - h + \mu_r h}, \tag{2.19}$$

$$b_1 = D' - \frac{D' - E' + F'h}{1 - h + \mu_r h}, \tag{2.20}$$

$$a_2 = \frac{\mu_r(D' - E') - F'(1-h)}{1 - h + \mu_r h}. \tag{2.21}$$

The membrane tension $\Sigma \approx \Sigma_0 + \epsilon^2\Sigma_1$ remains to be determined from the inextensibility (constant surface area) of the lipid membrane, which can be recast in terms of the incompressibility condition for the velocity $\boldsymbol{v}$ on the membrane

$$\boldsymbol{\nabla}_s \cdot \boldsymbol{v} = \epsilon\,(\partial_x u + h_x\partial_z u) + \epsilon^3\left(-(\partial_x h)^2\partial_x u + \partial_x h\partial_x w\right) + O(\epsilon^5) = 0. \tag{2.22}$$

At leading order the surface incompressibility gives

$$\left[\partial_x u + h_x\partial_z u\right]_{z=h} = \frac{\mathrm{d}}{\mathrm{d}x}u(x, z = h(x, t)) = 0, \tag{2.23}$$

which is the condition for the local membrane area conservation. In addition, the total surface area $\mathscr{L}$ is given by

$$\mathscr{L} \equiv \int_{-L/2}^{L/2}\sqrt{1+\epsilon^2 h_x^2}\mathrm{d}x \sim L + \frac{\epsilon^2}{2}\int_{-L/2}^{L/2} h_x^2\mathrm{d}x + O(\epsilon^4). \tag{2.24}$$

Consequently, at leading order $O(\epsilon^2)$, the constant excess area $\mathscr{L} - L$ implies

$$\mathscr{L} - L = \frac{\epsilon^2}{2}\int_{-L/2}^{L/2} h_x^2\mathrm{d}x \equiv \frac{\epsilon^2}{2}S = \text{constant}, \tag{2.25}$$

where S is the scaled excess area and L is the scaled length of the domain.

The constant excess area constraint determines the homogeneous membrane tension Σ_0, while the local area conservation (2.23) gives the gradient of the spatially inhomogeneous tension Σ_{1x} in terms of h and p_{2x}:

$$\Sigma_{1x} = \frac{1}{\bar{C}}\left[-(1-h)(g_x + \beta_{1x}) - p_{2x} + 2\beta_2\right] - \frac{2c_1(1+(-1+\mu_r)h)}{\bar{C}(1-h)h}, \tag{2.26}$$

where the constant $c_1 \equiv u(x, z = h(x, t))$ is from integrating (2.23). Consequently, the gradient of pressure p_2 can be expressed as

$$p_{2x} = \frac{(-1+h)^3(g_x + \beta_{1x}) + f_1}{(1-h)^3 + \mu_r h^3}, \tag{2.27}$$

where f_1 is a second integration constant obtained from integrating the equation that involves p_{2xx}. Inserting all this in (2.13), we obtain the evolution equation for h as

$$\partial_t h + \partial_x\left[-\frac{(-1+h)^3h^3(g_x+\beta_{1x}) + f_1h^3}{12\left((1-h)^3+\mu_r h^3\right)} + \frac{c_1 h}{2}\right] = 0. \tag{2.28}$$

In three dimensions, the evolution equation for $h(x, y, t)$ is

$$\partial_t h + \boldsymbol{\nabla}\cdot\left[-\frac{(-1+h)^3h^3\boldsymbol{\nabla}(G+\beta_1) + \boldsymbol{f}h^3}{12\left((1-h)^3+\mu_r h^3\right)} + \frac{\boldsymbol{c}h}{2}\right] = 0, \tag{2.29}$$

with $\boldsymbol{f} = (f_1, f_2)$, $\boldsymbol{c} = (c_1, c_2)$, $G \equiv \bar{C}\Sigma_0\nabla^2 h - \varkappa\nabla^4 h$ and $\boldsymbol{\nabla} \equiv (\partial_x, \partial_y)$. In the following we set the integration constants $\boldsymbol{f}$ and $\boldsymbol{c}$ zero as there is no imposed fluid flow at the

boundary in electroformation experiments (Angelova & Dimitrov 1986; Angelava & Dimitrov 1987).

At leading order the governing equation for the normal electric field strengths is given by (2.11). The trans-membrane potential $V_m \equiv \Phi_2 - \Phi_1|_{z=h} = E_2 h - v - E_1(h-1)$ satisfies (2.10). In the long-wave formulation, the convection terms vanish because we set the integration constant $u(z=h(x,t)) = c = 0$ in deriving the leading-order equations. As a result $\mathrm{d}/\mathrm{d}t \equiv \partial/\partial t + u\partial/\partial x = \partial/\partial t$ in (2.10) and (2.11). This is consistent with the assumption of vanishing charge convection on the membrane in the linear analyses for a flat tensionless membrane (Seiwert *et al.* 2012; Seiwert & Vlahovska 2013). Furthermore, the convection of the induced surface charge has been shown to have little effect on the electro-deformation of a viscous drop (Feng & Beard 1991).

Equations (2.28), (2.10) and (2.11), together with the integral constraint in (2.25), are the governing long-wave equations for an inextensible elastic membrane under an electric field. A complete list of dimensionless parameters and their meaning is given in table 1. In most electroformation experiments (Angelova & Dimitrov 1986; Angelava & Dimitrov 1987; van Swaay & deMello 2013), E_0 is often a few kilovolts per metre, h_0 is often of the order of millimetres, $\sigma_1 \sim 10^{-4}$ S m^{-1} and $\epsilon \leqslant 0.3$ (for a vesicle filling the channel $\epsilon = 2r_0/2\pi r_0 = 1/\pi \sim 0.3$). However, the lipid bilayer membrane remains intact for $E_0 \sim 30$ kV m^{-1}. Therefore the the range of physically realizable β is computed as $0 \leqslant \beta \leqslant 300$.

Six boundary conditions are needed to complete the problem formulation. In § 3 we will focus on periodic boundary conditions. For our governing long-wave equation, the periodic boundary conditions are closely related to the boundary conditions: $h_x = h_{xxx} = (g+\beta_1)_x = 0$ at $x = \pm L/2$ associated with multiple blisters for a thin film (Blount *et al.* 2012). For both the periodic and the multiple blister boundary conditions, the homogeneous membrane tension Σ_0 can be explicitly expressed in terms of h by taking the derivative of (2.25) with respect to time and performing integration by parts:

$$\Sigma_0 = \frac{\displaystyle\int_{-L/2}^{L/2} F h_{xxx}\left[\varkappa h_{xxxxx} - \frac{\beta}{2}(\varepsilon_r E_1^2 - E_2^2)_x\right]\mathrm{d}x}{\bar{C}\displaystyle\int_{-L/2}^{L/2} F h_{xxx}^2 \mathrm{d}x}, \tag{2.30}$$

where the function F is defined as

$$F = -\frac{(-1+h)^3 h^3}{12\left[(1-h)^3 + \mu_r h^3\right]}. \tag{2.31}$$

Summary of formulation

In this paper we focus on the two-dimensional system with periodic boundary conditions in the horizontal direction. The governing equations are (2.28), (2.10) and (2.11) with Σ_0 computed from (2.30). The horizontal velocity $u_i = (\mu_2/\mu_i)(\partial_x p_i/2)z^2 + a_i z + b_i$ depends on Σ_0 and Σ_1 through the coefficients in (2.19), (2.20) and (2.21) ($b_2 = 0$ from the no-slip condition at $z = 0$).

For a DC electric field, the displacement current $\mathrm{d}E_1/\mathrm{d}t$ (associated with charge relaxation on the surface) is small and often neglected because $\alpha \ll 1$. Setting $\alpha = 0$ in (2.11) gives $E_2 = \sigma_r E_1$, and (2.10) can be integrated to give

$$V_m = V_m(0) + \frac{1}{c_m \chi(t)}\int_0^t -\frac{\chi(t')}{(1-\sigma_r)h - 1}\mathrm{d}t', \tag{2.32}$$

https://doi.org/10.1017/jfm.2014.281 Published online by Cambridge University Press

Dimensionless variable	**Description**	
$g \equiv \bar{C}\Sigma_0 \partial_x^2 h - \varkappa \partial_x^4 h$	Membrane 'pressure'	
$V_m \equiv \Phi_1 - \Phi_2\|_{z=h}$	Trans-membrane potential	
$E_i \equiv \boldsymbol{n} \cdot \boldsymbol{E_i}$	Normal electric field	
$\Sigma \approx \Sigma_0 + \epsilon^2 \Sigma_1$	Membrane tension	
Dimensionless parameter	**Description**	**Value or range**
$\beta \equiv \varepsilon_2 E_0^2/[\mu_2\sigma_1/(h_0 C_m \epsilon^2)]$	Electric pressure scaled by $\mu_2\sigma_1/(h_0 C_m \epsilon^2)$	$0 \leqslant \beta \leqslant 300$
$\varkappa \equiv \kappa/[\mu_2\sigma_1 h_0^2/(2C_m\epsilon^6)]$	Bending modulus scaled by $\mu_2\sigma_1 h_0^2/(2C_m\epsilon^6)$	$\varkappa \ll 1$ in most cases
$\bar{C} \equiv \gamma_0/[\mu_2\sigma_1/(2C_m\epsilon^4)]$	Membrane tension scaled by $\mu_2\sigma_1/(2C_m\epsilon^4)$	$\bar{C} = 1$ in this work
$g_m \equiv (G_m h_0)/\sigma_1$	Membrane conductance scaled by σ_1/h_0	$0 \leqslant g_m \leqslant\sim O(1)$
$\alpha \equiv \varepsilon_1/(h_0 C_m)$	Ratio of bulk to membrane charging times	$\alpha \ll 1$
$\mu_r \equiv \mu_1/\mu_2$	Viscosity ratio	$\mu_r = 1$ in this work
$\varepsilon_r \equiv \varepsilon_1/\varepsilon_2$	Permittivity ratio	$\varepsilon_r = 1$ in this work
$\sigma_r \equiv \sigma_1/\sigma_2$	Conductivity ratio	$1 \leqslant \sigma_r \leqslant 50$
$S \equiv \int_{-L/2}^{L/2} (h_x)^2 \mathrm{d}x$	Excess length in two dimensions	$S < 1$ in this work

TABLE 1. Dimensionless variables and parameters.

$$\chi(t) = \exp\left(\frac{g_m t}{c_m} - \frac{1}{c_m}\int_0^t \frac{1}{(1-\sigma_r)h - 1}\mathrm{d}t'\right). \tag{2.33}$$

In the absence of membrane conductance ($g_m = 0$), the above equation can be easily recast to give

$$E_1(x,t) = E_1(x,0)\frac{-1+(1-\sigma_r)h(x,0)}{-1+(1-\sigma_r)h(x,t)}\mathrm{e}^{I(t)}, \tag{2.34}$$

with

$$I(t) = \frac{1}{c_m}\int_0^t \frac{1}{-1+(1-\sigma_r)h(t')}\mathrm{d}t'. \tag{2.35}$$

It can be easily seen that $I(t) < 0$ as long as $\sigma_r \geqslant 0$ and $0 < h < 1$. Therefore the electric field $E_1 \to 0$ as the non-conducting capacitive membrane charges over time.

2.2. *Equilibrium profile for a non-conducting membrane ($g_m = 0$) in DC fields*

For a non-conducting membrane ($g_m = 0$) in a DC electric field ($\alpha = 0$), the following analysis gives admissible equilibrium profiles determined by the volume (area) under the membrane and the total area (length) of the two-dimensional (one-dimensional) membrane. No such simple equilibrium results are available for a conducting membrane ($g_m > 0$) or in an AC electric field (ν is a function of time).

For a non-conducting ($g_m = 0$) capacitive membrane in a DC field, the normal electric fields E_1 and E_2 decay exponentially to zero as the membrane charges up (see (2.34) and (2.35)). At equilibrium the profile satisfies the simple equation

$$\frac{\mathrm{d}}{\mathrm{d}x}\left[F\frac{\mathrm{d}g}{\mathrm{d}x}\right] = 0 \tag{2.36}$$

for $x \in (-L/2, L/2)$ with either (i) periodic boundary conditions, or (ii) $h_x = h_{xxx} = g_x = 0$ at $x = \pm L/2$. The function F (2.31) is non-zero as long as $0 < h < 1$. In addition the leading-order excess length of the interface and area (or volume in three dimensions) under the interface remain constant:

$$\int_{-L/2}^{L/2}(h_x)^2\mathrm{d}x = S = \text{constant}, \qquad \int_{-L/2}^{L/2} h\mathrm{d}x \equiv \theta = \text{constant}. \tag{2.37}$$

Integrating (2.36) once and setting the integration constant to zero, we obtain

$$\frac{\mathrm{d}}{\mathrm{d}x}\left[\bar{C}\Sigma_0\frac{\mathrm{d}^2h}{\mathrm{d}x^2} - \varkappa\frac{\mathrm{d}^4h}{\mathrm{d}x^4}\right] = 0. \tag{2.38}$$

For periodic boundary conditions, the equilibrium profile takes the form

$$h = a\cos\left(\frac{2n\pi x}{L}\right) + b\sin\left(\frac{2n\pi x}{L}\right) + \frac{\theta}{L}, \tag{2.39}$$

where integer n and membrane tension Σ_0 are related via $n^2 = -(\bar{C}\Sigma_0/\varkappa)(L/2\pi)^2$ and $\Sigma_0 < 0$. Here a and b are related to S via $(2n\pi/L)^2((a^2+b^2)L)/2 = S$. For $h_x = h_{xxx} = g_x = 0$ at $x = \pm L/2$, the equilibrium profile in (2.39) splits into a symmetric profile

$$h(x) = \pm\frac{\sqrt{2S/L}}{2N\pi/L}\cos\left(\frac{2N\pi x}{L}\right) + \frac{\theta}{L}, \tag{2.40}$$

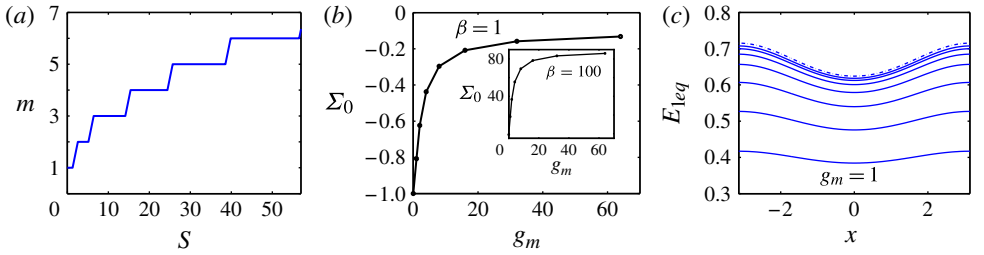

FIGURE 2. (Colour online) (*a*) Equilibrium mode number as a function of excess length S for $\theta/L = 1/2$. (*b*) Equilibrium membrane tension as a function of membrane conductance from simulations with $\beta = 1, S = 6.2995$ and parameters $(\varepsilon_r, \sigma_r, \mu_r, \varkappa) = (1, 2, 1, 1)$; $\beta = 100$ for the inset. (*c*) The corresponding equilibrium electric field profile E_{1eq} as the membrane conductance increases (with a multiple of 2) from bottom ($g_m = 1$) to top ($g_m = \infty$ for the dashed line).

and an antisymmetric profile

$$h(x) = \pm\frac{\sqrt{2S/L}}{2N\pi/L}\sin\left(\frac{2N\pi x}{L}\right) + \frac{\theta}{L} \tag{2.41}$$

with $N^2 = -(\bar{C}\Sigma_0/\varkappa)(L/2\pi)^2$. Here N is an integer for the symmetric profile, and a half-integer for the antisymmetric profile.

For a given membrane excess length S and an area θ under the membrane in two dimensions, m has to satisfy the following inequalities (from $0 < h < 1$):

$$0 < -\frac{\sqrt{2S/L}}{2m\pi/L} + \frac{\theta}{L}, \quad \frac{\sqrt{2S/L}}{2m\pi/L} + \frac{\theta}{L} < 1, \tag{2.42}$$

with $m = n$ for the periodic boundary conditions and $m = N$ for the blistering boundary conditions. The corresponding total energy of the membrane interface is computed as

$$\mathscr{E} = \varkappa\int_{-L/2}^{L/2}(h_{xx})^2\,\mathrm{d}x + \Sigma_0\bar{C}S = \left(\frac{2m\pi}{L}\right)^2\varkappa S. \tag{2.43}$$

The most stable equilibrium will be given by one of the plausible values of m that minimizes the membrane energy in (2.43). Figure 2(*a*) illustrates the variation of m with S for $\theta/L = 1/2$. For a capacitive membrane with conductance, no such simple expression for the equilibrium profile was found because of the nonlinearity from the non-vanishing E at equilibrium. For a conducting membrane ($g_m > 0$) we compute the steady equilibrium profiles numerically using a semi-implicit spectral code explained in § 2.4. The same equilibrium membrane sinusoidal profiles are found in a periodic domain as when $g_m = 0$. However the membrane tension is no longer negative for large membrane conductance g_m and large electric field strength β, see figure 2(*b*). In addition, figure 2(*c*) shows that E_1 reaches an asymptotic profile in the large membrane-conductance limit.

2.3. *Linear stability of a tensionless flat membrane in a DC field*

Linear stability analysis on a flat capacitive conducting tension-free membrane has been conducted for both DC (Seiwert *et al.* 2012) and AC (Seiwert & Vlahovska 2013) fields. In contrast to the stability of a fluid interface that depends solely on

the mismatch of the fluid dielectric properties (see Craster & Matar 2005; Roberts & Kumar 2009), the membrane conductance is found to be essential for the linear instability (Seiwert *et al.* 2012), while the linear growth rate is reduced by the electric field frequency in the AC field (Seiwert & Vlahovska 2013). Here we will examine the linear stability of a flat membrane in a DC field.

We linearize the long-wave equations around the flat base state

$$h_0 = \text{constant}, \quad E_{1,0} = \frac{g_m}{1 + g_m[\sigma_r h_0 + (1 - h_0)]}, \quad E_{2,0} = \sigma_r E_{1,0}. \tag{2.44}$$

The perturbed membrane profile can be written as $h(x, t) = h_0 + \delta h \exp(\mathrm{i}Qx + \lambda t)$ (with Q the wavenumber and λ the growth rate) with similar expressions for E_1 and E_2. Focusing on the DC field ($\alpha = 0$ and $\nu = 1$) case, we substitute the perturbed h, E_1 and E_2 into the long-wave model (2.10), (2.11) and (2.28) and linearize the equations with respect to perturbations (δh, δE_1 and δE_2) around the base state. In the long-wave formulation the membrane tension responds to the bending and electric forces (2.30) to keep the membrane inextensible. For a tensionless membrane, an analytical form for the growth rate can be found as

$$\lambda \approx \frac{\beta\left(\varepsilon_r - \sigma_r^2\right)(1 - \sigma_r) g_m^3}{96(1 + \mu_r)\left[1 + (\sigma_r + 1) g_m/2\right]^3} Q^2 - \frac{\varkappa}{96(1 + \mu_r)} Q^6, \tag{2.45}$$

with $h_0 = 1/2$. From (2.45) the maximum growth rate (λ_{max}) and the corresponding wavenumber Q_{max} can be computed as

$$Q_{max} = \left[\frac{\beta(\varepsilon_r - \sigma_r^2)(1 - \sigma_r)}{3\varkappa}\left(\frac{g_m}{\left(1 + \frac{\sigma_r + 1}{2} g_m\right)}\right)^3\right]^{1/4} \sim \varkappa^{-1/4}, \tag{2.46}$$

$$\lambda_{max} = \frac{\beta\left(\varepsilon_r - \sigma_r^2\right)(1 - \sigma_r) g_m^3}{144(1 + \mu_r)\left[1 + (\sigma_r + 1) g_m/2\right]^3} Q_{max}^2 \sim \varkappa^{-1/2}. \tag{2.47}$$

In the limit of large membrane conductance $g_m \to \infty$,

$$Q_{max} \to \left[\frac{8\beta(\varepsilon_r - \sigma_r^2)(1 - \sigma_r)}{3\varkappa(\sigma_r + 1)^3}\right]^{1/4}, \quad \lambda_{max} \to \frac{\beta\left(\varepsilon_r - \sigma_r^2\right)(1 - \sigma_r)}{18(1 + \mu_r)(\sigma_r + 1)^3} Q_{max}^2. \tag{2.48}$$

In (2.45) the wavenumber dependence of the destabilizing component of the growth rate is quadratic, while a cubic dependence is reported in Ziebert *et al.* (2010), Ziebert & Lacoste (2011) and Seiwert *et al.* (2012). This difference can be attributed to the spatial variation of the electric potential: for a finite domain the electric potential varies linearly, while the electric potential decays exponentially with distance to the membrane in free space (Ziebert *et al.* 2010; Seiwert *et al.* 2012). Comparisons of predictions between the two models for the AC case would be expected to be similar to the DC case: the condition for instability $(\varepsilon_r - \sigma_r^2)(1 - \sigma_r) g_m > 0$ is the same as Seiwert *et al.* (2012)'s result; however the wavenumber dependence is different. Seiwert & Vlahovska (2013) conducted a thorough Floquet analysis for a membrane under an AC field in free space. We expect the same dependence of the linear stability on the physical parameters, and expect to see the difference in the dispersion for small q between a free space and a finite channel. But we defer the Floquet analysis on the long-wave equations for a membrane in an AC field to a future study, and instead focus on using numerical code to study both the linear stability (§ 3.1) and nonlinear dynamics (§ 3.2) of a lipid bilayer membrane under an AC field.

2.4. *Numerical implementation*

The evolution equation for the membrane height (2.28) is a sixth-order nonlinear differential equation. As a result, an explicit time-marching scheme has stringent stability constraints and it will be impractical to simulate the physics even in the one-dimensional case. To overcome the restriction on time-step, we formulate a semi-implicit scheme similar to that of Veerapaneni *et al.* (2009). In this scheme, the tension is treated explicitly and the terms with highest-order derivatives in (2.28) are treated implicitly. Suppose we have evolved the membrane position until $n\triangle t$ and we need to march to $(n+1)\Delta t$. First, we compute the tension Σ_0 at the nth level using (2.30) as

$$\Sigma_0^n \sim \frac{(S^n - S^0)/\Delta t + \displaystyle\int_{-L/2}^{L/2} Fh_{xxx}\left[\varkappa h_{xxxxx} - \frac{\beta}{2}(\varepsilon_r E_1^2 - E_2^2)_x\right] \mathrm{d}x}{\bar{C}\displaystyle\int_{-L/2}^{L/2} Fh_{xxx}^2 \mathrm{d}x}, \tag{2.49}$$

where Δt is the time step, S^0 is the initial excess area and S^n is the excess area in (2.37) evaluated with h^n at time $n\Delta t$. The term $(S^n - S^0)/\Delta t$ in the numerator is the penalty term that adjusts the tension based on the deviation of membrane area from the initial value S^0. A similar term has been used for simulating an inextensible elastic filament (Tornberg & Shelley 2004). Second, the membrane position is updated via a semi-implicit time-step as

$$h^{n+1} + \Delta t\left[F^n\left(\bar{C}\Sigma_0^n h_{xx}^{n+1} - \varkappa h_{xxxx}^{n+1}\right)_x\right]_x = h^n - \Delta t\left[F^n\frac{\beta}{2}\left(\varepsilon_r (E_1^n)^2 - (E_2^n)^2\right)\right]_x, \tag{2.50}$$

where $F^n \equiv F(h^n)$. Third, the evolution equation for the electric field E_1 (2.11) is discretized as

$$\begin{aligned}&\left(1 + \frac{g_m}{c_m}\Delta t\right)\left[(E_1^n - E_2^n)h^{n+1} - E_1^{n+1}\right] - \frac{\alpha}{c_m}E_1^{n+1}\\ &\quad = \left(\frac{\Delta t}{c_m} - \frac{\alpha}{c_m} - 1\right)E_1^n + \left(E_1^n - E_2^n\right)h^n - \Delta t\left(\nu' + \frac{g_m}{c_m}\nu\right).\end{aligned} \tag{2.51}$$

Here $E_2^{n+1} = \sigma_r E_1^{n+1}$ for $\alpha = 0$; for $\alpha \neq 0$ we update the electric field E_2 by solving the discretized evolution equation

$$E_2^{n+1} = \frac{\varepsilon_r \Delta t}{\alpha}\left[\left(1 - \frac{\alpha}{\Delta t}\right)E_1^n + \frac{\alpha}{\Delta t}E_1^{n+1} - \left(\frac{1}{\sigma_r} - \frac{\alpha}{\varepsilon_r \Delta t}\right)E_2^n\right]. \tag{2.52}$$

We solve for h^{n+1}, E_1^{n+1} and E_2^{n+1} simultaneously using the GMRES method (MATLAB 2012).

For the periodic boundary conditions the spatial derivatives are computed using the spectral collocation method (Canuto *et al.* 1986). Appropriate Δt and grid spacing Δx are chosen to keep the error in excess length S smaller than 0.1 % of the initial excess length throughout the simulations. In the following we focus on periodic boundary conditions with $L = 2\pi$ unless otherwise specified.

The code is validated to be second-order in time and spectral in space. Note that as a check we have numerically recovered the analytical equilibrium profiles for a non-conducting membrane ($g_m = 0$) in a DC field. We should also note that for a

conducting membrane in a DC field, the same equilibrium profiles as in the non-conducting case are numerically found for a given combination of (θ, S) but now the equilibrium membrane tension Σ_0 depends on the membrane conductance g_m as shown in figure 2(*b*). In the inset of figure 2(*b*) we show Σ_0 versus g_m for $\beta = 100$. Here $\Sigma_0 = -1$ when $g_m = 0$, and Σ_0 increases to positive values for large g_m. Figure 2(*c*) shows the equilibrium profile for the electric field E_{1eq} as the membrane conductance increases from bottom to top and in particular it shows that there is an asymptotic profile as g_m increases.

3. Results

Seiwert & Vlahovska (2013) quantified the linear instability of a tensionless flat membrane in free space in terms of membrane conductance g_m, mismatch of fluid dielectric permittivity ε_r and conductivity σ_r, electric capillary number Ca and electric field frequency ω. In our long-wave formulation the time scale is based on the membrane charging time ($c_m = 1$), and as a result their dimensionless (starred) parameters are related to ours as: $Ca^* = (2\varepsilon_r\beta/\varkappa)\epsilon$, $\xi^* = (\bar{C}/\varkappa)\epsilon^2$, and $\beta^* = (\varepsilon_r\beta\mu_r)/\epsilon^{-3}$.

In § 3.1 we focus on the linear growth rate from numerical simulations for a tensionless flat membrane in both DC and AC fields. Based on the linear results we perform simulations to investigate the nonlinear dynamics of the membrane at different values of β in § 3.2 and excess length in § 3.3. In § 3.4 we demonstrate the alternating travelling wave on an inextensible membrane under an AC field. All the results are presented with $T = t/(2\pi/\omega)$, the time scaled to the period of the underlying AC field, to help reveal the underlying mechanisms. Results from numerical explorations show that the nonlinear dynamics reported below can be found for a wide range of physical parameters. Thus the choice of parameter combinations in §§ 3.2–3.4 is made based on the physical realizability in the laboratory.

3.1. *Linear stability of a tensionless flat membrane in an electric field*

Seiwert & Vlahovska (2013)'s Floquet analysis shows that both membrane conductance g_m and small values of the AC field frequency ω destabilize the planar membrane, while the linear growth rate is decreased by large ω. Here we first present numerical results to validate our code against the linear growth rate (2.45) for a tensionless, flat membrane in DC electric field. We then present some numerical results to qualitatively compare with the Floquet results in figures 3 and 4 of Seiwert & Vlahovska (2013).

For the following results the initial conditions $h(x, 0) = 0.5 + 0.01\cos(Qx)$ and $E_1 = E_2 = 0$ are used in the numerical simulations. Figure 3(*a*) shows the linear growth rate for a tensionless flat membrane under a DC field with $(\varepsilon_r, \sigma_r, \mu_r, g_m, \varkappa, \alpha) = (1, 10, 1, 1, 300, 0)$. The solid curve is from (2.45), and the symbols are computed from the time evolution of the Fourier transform of h from numerical simulations with the same parameters. Figure 3(*b*) shows the growth rate for a tensionless flat membrane under an AC field (symbols joined by the dashed line) with $\omega = 0.75$, $v(t) = \sqrt{2}\sin(\omega t)$ and $(\varepsilon_r, \sigma_r, \mu_r, g_m, \varkappa, \alpha) = (1, 10, 1, 1.25, 10^{-2}, 0.1)$. The solid curve is the DC growth rate from (2.45) with the same parameters. Figure 3(*c*) shows the dependence of the growth rate on the AC field frequency (symbols joined by the dashed line) for $Q = 3.25$, $(\varepsilon_r, \sigma_r, \mu_r, g_m, \varkappa, \alpha) = (1, 10, 1, 1.25, 10^{-2}, 0.1)$ and $v(t) = \sqrt{2}\sin(\omega t)$.

Our dimensionless frequency ω is the same as that in Seiwert & Vlahovska (2013) as we use the membrane charging time for the time unit. The electric potential for

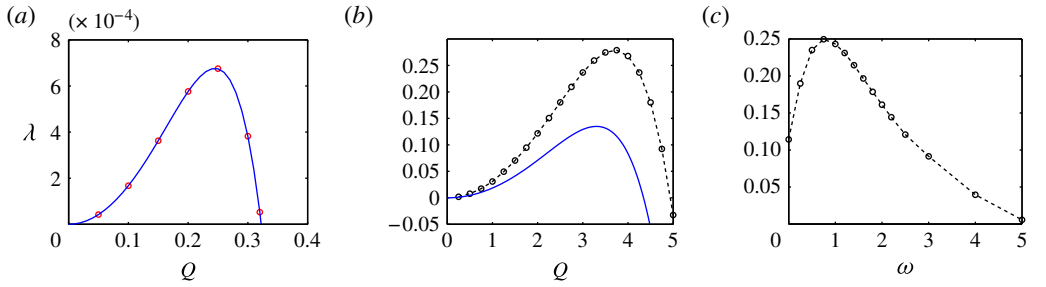

FIGURE 3. (Colour online) Linear growth rate λ for a tensionless flat membrane with $\beta = 1$. Solid curves are λ from (2.45) for a non-conducting membrane under a DC field, and symbols are from simulations. (*a*) Linear growth rate λ versus Q in a DC field with $(\varepsilon_r, \sigma_r, \mu_r, g_m, \varkappa, \alpha) = (1, 10, 1, 1, 300, 0)$. (*b*) λ versus Q in an AC field with $\omega = 0.75$, $v = \sqrt{2}\sin(\omega t)$, $(\varepsilon_r, \sigma_r, \mu_r, g_m, \varkappa, \alpha) = (1, 10, 1, 1.25, 10^{-2}, 0.1)$. (*c*) λ versus ω for $Q = 3.25$ and $(\varepsilon_r, \sigma_r, \mu_r, g_m, \varkappa, \alpha) = (1, 10, 1, 1.25, 10^{-2}, 0.1)$.

the base state is for an infinite domain in Seiwert & Vlahovska (2013), while for our analysis the base-state electric potential is for a finite domain. As a result we focus on qualitative comparison here. The growth rate versus ω in figure 3(*c*) is in qualitative agreement with figure 3 of Seiwert & Vlahovska (2013): the linear growth rate decreases to zero as the frequency increases. The wavenumber dependence in figure 3(*b*) is also in qualitative agreement with results in figure 4 of Seiwert & Vlahovska (2013). Here $\beta = 1$ is used for results in figure 3. For a different value of β we expect a similar dispersion curve with a maximum growth rate proportional to $\beta^{3/2}$ from the linear analysis for a non-conducting tensionless membrane.

3.2. *Effects of AC field magnitude* β

In this subsection we fix $\omega = 0.75$, $L = \pi/Q$ with $Q = 3.3$, $(\varepsilon_r, \sigma_r, \mu_r, g_m, \varkappa, \alpha) = (1, 60, 1, 1.25, 10^{-2}, 0.1)$ and $v(t) = \sqrt{2}\sin(\omega t)$. The excess length is fixed at $S = 0.141$ as the electric field strength β is increased. These parameters are realizable in the laboratory, therefore the nonlinear dynamics reported here is potentially observable in an experiment.

Figure 4 shows the membrane dynamics over one period of oscillation. Under an AC electric field, most of the time the membrane stays close to the equilibrium shape under a DC field determined by the excess length S and the volume θ ($S = 0.141$ and $\theta = 0.5$ in this subsection). However, when the electric potential approaches its mean (zero in this subsection), the membrane undergoes fast dynamics that depends on β. For $\beta = 50$ (figure 4*a,b*) a fast temporal membrane undulation is found around $v = 0$. For $\beta = 200$ (figure 4*c,d*) the fast membrane undulation leads to flip-flop of the membrane profile from h to $1 - h$. Figures 4(*b*) and 4(*d*) show the membrane height at $x = 0$ versus time (solid curves) with the dashed curves for the electric potential $v(t)$.

The corresponding temporal variation of the membrane tension is shown in figure 5(*a,b,c*): (*a*) shows Σ_0 for different values of β; (*b*) and (*c*) show the correlation between Σ_0 and $\langle H^2 \rangle = \int_{-L}^{L} H^2 \mathrm{d}x$ near the minimum of Σ_0 for $\beta = 50$ and $\beta = 200$, respectively. For every half a cycle the membrane tension Σ_0 reaches minima (solid curves in figure 5*b,c*), whereas the membrane deformation reaches maxima (dashed

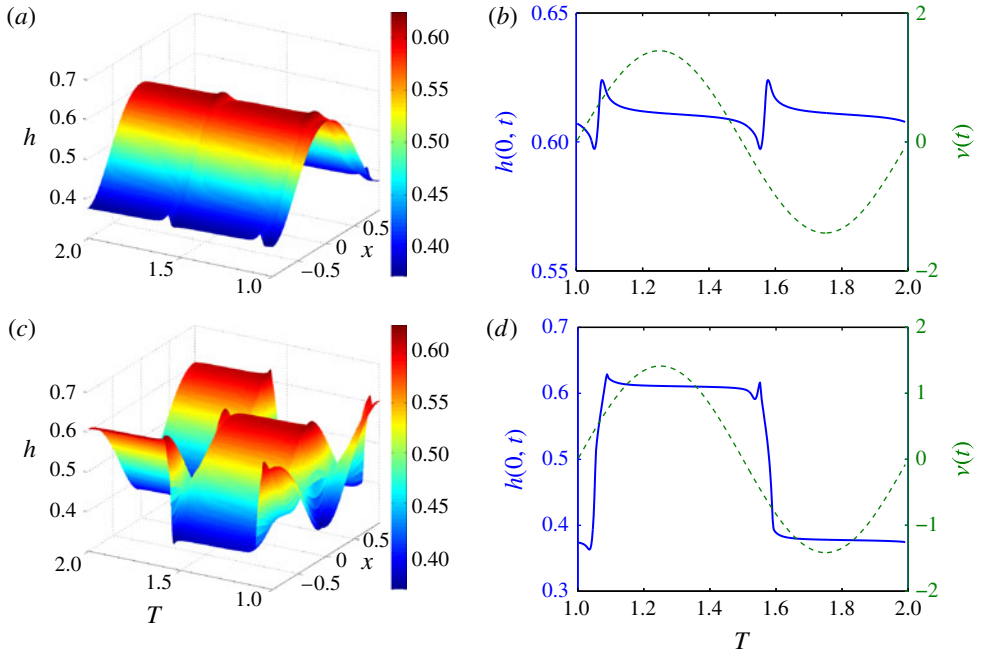

FIGURE 4. (Colour online) Membrane dynamics over one period for $(\varepsilon_r, \sigma_r, \mu_r, g_m, \varkappa, \alpha) = (1, 60, 1, 1.25, 10^{-2}, 0.1)$, $\omega = 0.75$, and $\nu(t) = \sqrt{2}\sin(\omega t)$ is the dashed line in (*b*) and (*d*); (*a,b*) $\beta = 50$ and (*c,d*) $\beta = 200$. (*a,c*) Time–space plot of h; (*b,d*) the membrane height at $x = 0$ over one period.

lines in figure 5(*b,c*). This is clearly illustrated by the concurrence of the maxima in $\langle H^2 \rangle$ and the minimum in Σ_0 in figure 5(*a,b,c*).

Figure 5(*d,e*) shows the variation in the surface-induced charge density q and the trans-membrane potential V_m from $T = 1.5$ to $T = 1.6$. Depending on whether the membrane flip-flops (high β) or undulates (low β) when Σ_0 is close to minimum, the distributions of q and V_m also vary with time differently. As T increases from 1.5 to 1.6 from the bottom to the top in figure 5(*d*), we observe the same surface charge distribution between $\beta = 50$ (dashed curves for undulating) and $\beta = 200$ (solid curves for flip-flopping) before $T = 1.55$ After $T = 1.56$, substantial differences in both q and V_m are observed between the two cases. In particular, as the membrane flip-flops the trans-membrane potential at the centre ($x = 0$) switches from maximum to minimum.

The above results show that the nonlinear dynamics of an inextensible elastic membrane in an AC field is closely related to the temporal variation of membrane tension Σ_0, which is in synchrony with the external AC field $\nu(t)$ for small and moderate S. (See figure 6(*b*) for the effects of S on the correlation between Σ_0 and $\nu(t)$.) The membrane deformation gets amplified when Σ_0 is around the minimum and $\nu(t)$ is around its mean. This may be understood by the linear instability of a tensionless membrane: when Σ_0 is close to zero the tensionless membrane is linearly unstable for $(\varepsilon_r - \sigma_r^2)(1 - \sigma_r)g_m > 0$. At large β the undulation of the membrane is replaced by the flip-flop of the membrane profile, and we observe overshoot in membrane height at $x = 0$ before and after the flip-flop. In addition we find higher

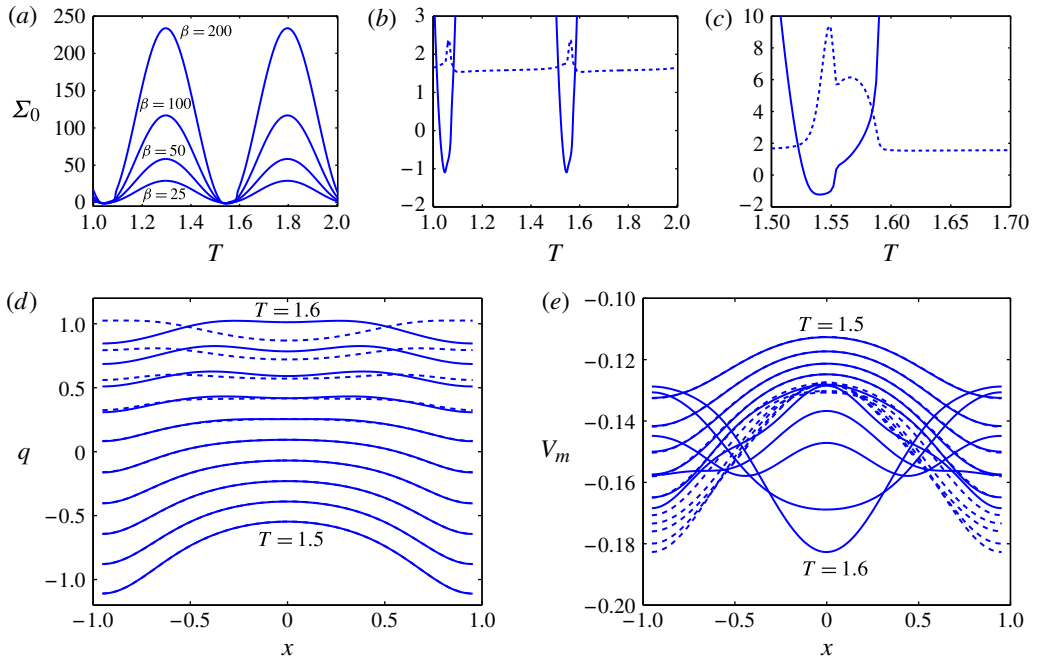

FIGURE 5. (Colour online) (*a*) Membrane tension Σ_0 over one period for $\beta = 25$, 50, 100 and 200. (*b*) Σ_0 (solid line) for $\beta = 50$ and $\langle H^2 \rangle \equiv \int_{-L}^{L} H^2 \mathrm{d}x$ (dashed line). (*c*) As (*b*) but for $\beta = 200$. (*d*,*e*) Dynamics of the induced surface charge q (*d*) and trans-membrane potential V_m (*e*) from $T = 1.5$ to $T = 1.6$ with $\Delta T = 0.01$ between two curves; $\beta = 50$ for dashed curves and $\beta = 200$ for solid curves.

surface charge density at $x = 0$ in figure 5(*d*), where the membrane height overshoots the most before and after the flip-flop (see figure 4).

At other times when Σ_0 is large, the membrane profile stays close to the analytic equilibrium membrane profile under a DC field. From simulations for higher membrane conductance we find that while membrane undulation still gets amplified when $\Sigma_0 \sim 0$, a higher electric field is needed for the membrane flip-flop.

The same nonlinear dynamics of membrane undulation and flip-flop under an AC field can be observed for other parameter combinations, such as $(\varepsilon_r, \sigma_r, \mu_r, g_m, \varkappa, \alpha) = (1, 10, 1, 1.25, 10^{-2}, 0.1)$. As the linear growth rate depends on β, σ_r and ε_r, it is reasonable to expect (and indeed we observe numerically) that higher β is needed to see the same nonlinear membrane dynamics when σ_r is decreased. For example, both the undulation and membrane flip-flop dynamics can be observed for $(\varepsilon_r, \sigma_r, \mu_r, g_m, \varkappa, \alpha) = (1, 10, 1, 0.01, 10^{-2}, 0.1)$ when β is increased to several thousand.

3.3. *Nonlinear dynamics at different excess length S*

Here we investigate how membrane flip-flopping dynamics under a strong AC electric field may depend on the membrane excess length S. Figure 6(*a*) shows the variation of membrane height at $x = 0$ for four values of S (see caption). At $\beta = 200$ we observe an overshoot in membrane height and the associated membrane flip-flopping for all four values of S. In addition we find that the overshoot in membrane height (when

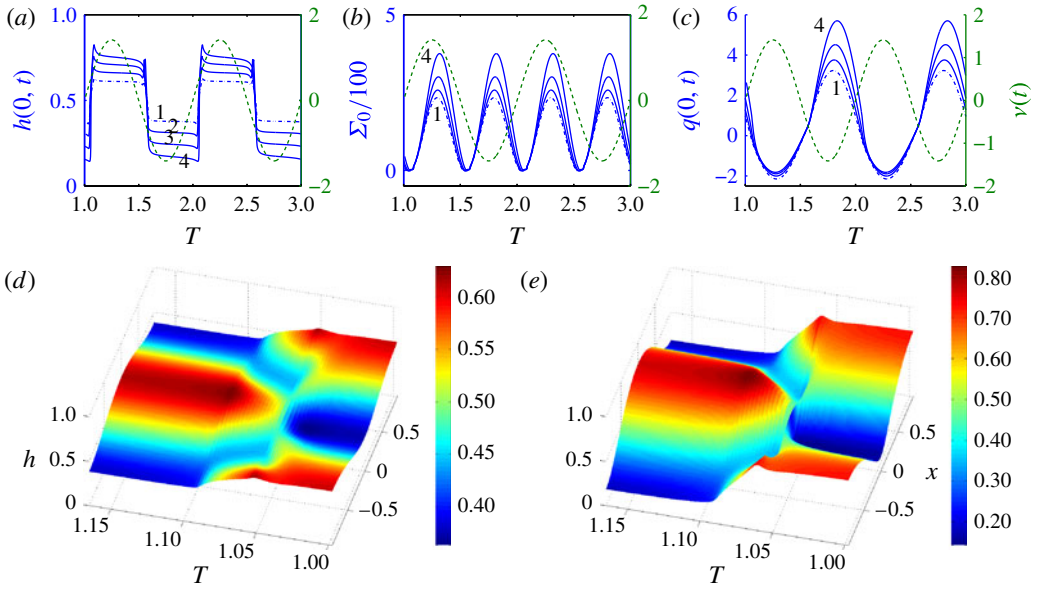

FIGURE 6. (Colour online) Flip-flopping dynamics of membrane with different excess length: $S = 0.141,\ 0.3172,\ 0.564,\ 0.8812$ for curves 1, 2, 3, and 4, respectively; $\beta = 200$, $\omega = 0.75$, $\nu(t) = \sqrt{2}\sin(\omega t)$ (dashed line) and $(\varepsilon_r,\ \sigma_r,\ \mu_r,\ g_m,\ \varkappa,\ \alpha) = (1,\ 60,\ 1,\ 1.25,\ 10^{-2},\ 0.1)$. (*a–c*) Temporal variation of h, Σ_0 and q at $x = 0$. (*d,e*) Flip-flopping of h for $S = 0.141$ (*d*) and $S = 0.8812$ (*e*) when $\Sigma_0 \sim 0$.

Σ_0 is close to zero, around its minimum) is enhanced as the excess length S increases from 0.141 to 0.8812, as shown in figure 6(*a*). Figure 6(*b*,*c*) shows the corresponding variation of Σ_0 and q at $x = 0$, where we see $\Sigma_0 \sim 0$ every half a cycle, corresponding to the overshoot in membrane height in figure 6(*a*). From figure 6(*b*) we note that the magnitude of Σ_0 increases with increasing S. Figure 6(*d*,*e*) shows space–time plots of the membrane profile when the membrane flip-flops.

We also observe from figure 6(*b*) that, even though the membrane flip-flops every half a cycle when $\Sigma_0 \sim 0$, the membrane height overshoots more when ν is positive. When ν is negative, Σ_0 reaches a maximum and therefore stabilizes the membrane and suppresses the overshoot before and after the flip-flop. Such asymmetry between the $\nu > 0$ half-cycle and the $\nu < 0$ half-cycle is also reflected in the surface charge density: the S dependence of q is amplified when $\nu < 0$ (figure 6*c*).

The corresponding space–time plots for q and V_m for two values of S are shown in figure 7, where we observe that the trans-membrane potential is out of phase with q. As S increases, we observe that the charge density will focus more at $x = 0$ around $T \sim 1.8$, just before the sudden overshoot in the membrane height and the fast change in V_m at $T \sim 2$. In addition we observe the trans-membrane potential at $x = 0$ has fast temporal variation when the membrane height flip-flops during the positive half-cycles. During the negative half-cycles, V_m has fast temporal variation at the end points.

3.4. *Nonlinear 'travelling' wave on an inextensible elastic membrane*

Numerical exploration shows that under strong electric field the nonlinear dynamics of a membrane with a sufficiently large excess length S is no longer the periodic

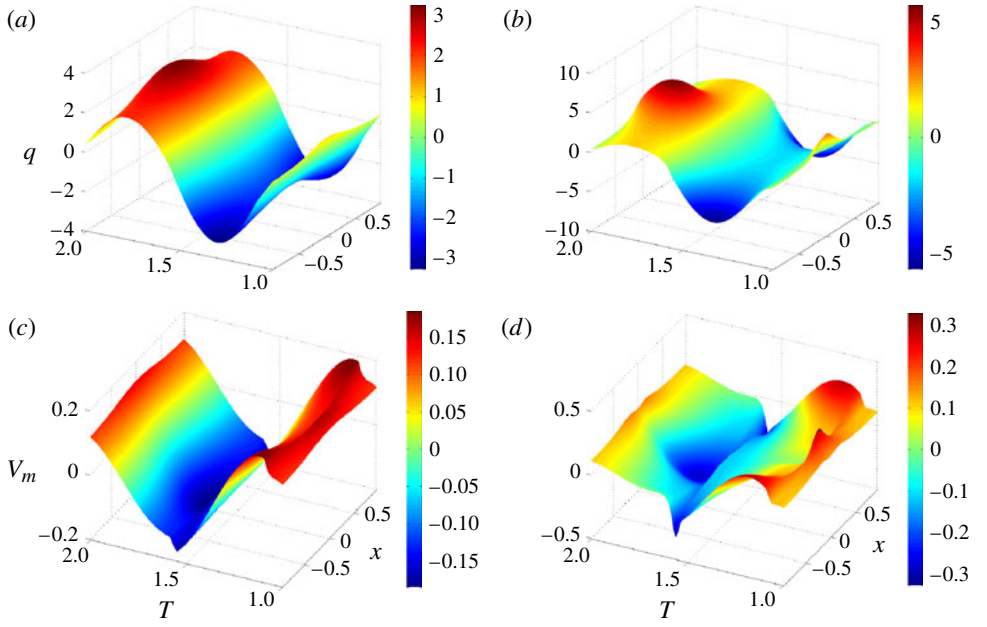

FIGURE 7. (Colour online) Variation of surface charge (a,b) and trans-membrane potential (c,d) from the simulations in figure 6; $S = 0.141$ for (a,c), and $S = 0.8812$ for (b,d).

undulation or membrane flip-flop discussed in §§ 3.2 and 3.3. Here we present an example from simulations for $S = 0.1138$, $\theta = 0.2$, $\beta = 300$, $(\varepsilon_r, \sigma_r, \mu_r, g_m, \varkappa, \alpha) = (1, 60, 1, 0.01, 10^{-6}, 0.1)$, $\omega = 0.1\pi$ and $v(t) = \sqrt{3}/2 + (\sqrt{2}/2)\sin(\omega t)$; 256 modes and $\Delta t = 1/100$ are used in the simulations.

In this example the membrane is placed closer to the bottom electrode ($\theta = 0.2$), which is similar to the experimental setup for electroformation. At the beginning the membrane undergoes undulation when Σ_0 approaches a minimum. Very quickly the translational symmetry is broken and a lateral net movement (from right to left in this case) develops due to the initial condition, which is $h(x, 0) = 0.2 + 0.15\cos(x) + 0.015(\cos(5x) + \sin(6x))$. We find opposite movement (from left to right) if the initial condition is inverted.

The temporal variation of Σ_0 (solid line) and $\langle H^2 \rangle$ (dashed line) is shown in figure 8(a), which illustrates the correlation between maxima in $\langle H^2 \rangle$ and minima in Σ_0. Figure 8(b) shows the membrane height at $x = 0$ (solid line) versus time for five periods. The corresponding charge density is shown in figure 8(c). The dashed line in figures 8(b, c) is the electric potential $v(t)$. Again Σ_0 reaches a minimum when v reaches its mean. While the tension Σ_0 remains positive within a cycle, a larger maximum is reached in the first half-cycle than the second in 8(a). The variation of membrane height at $x = 0$ with T in 8(b) shows that a maximum height is reached every half a cycle, with a clear indication of double-periodic dynamics. In 8(c) the surface charge density q at $x = 0$ oscillates with the same periodicity T but with a slightly decreasing amplitude. Figure 8(d–f) shows time–space plots for h, q and V_m, respectively, over one period from $T = 59$ to $T = 60$.

Figure 9 shows the lateral membrane movement. In figure 9(a–c) we show the profiles of h, q and V_m at multiples of the period from $T = 31$ (dashed curve) to

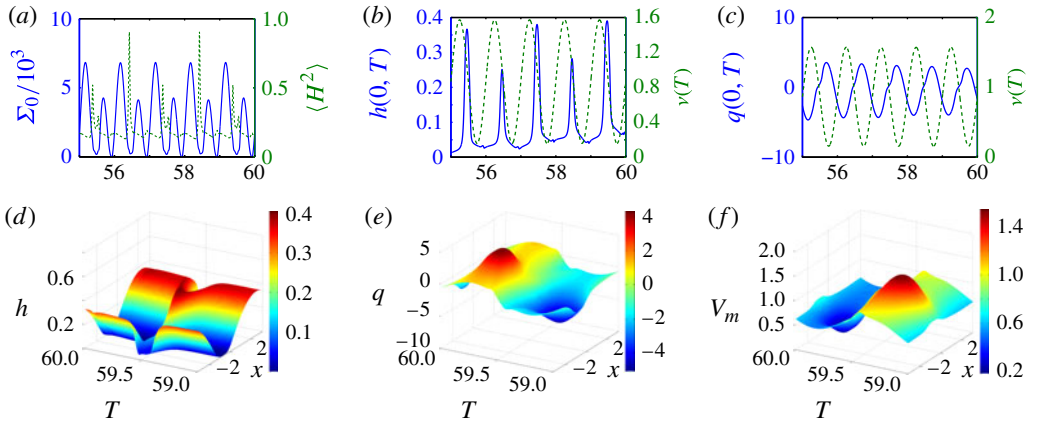

FIGURE 8. (Colour online) Non-periodic dynamics for $S=0.1138$, $\theta=0.2$, $\beta=300$, $\omega=0.1\pi$, $\nu(t)=\sqrt{3}/2+(\sqrt{2}/2)\sin(\omega t)$ and $(\varepsilon_r, \sigma_r, \mu_r, g_m, \varkappa, \alpha)=(1, 60, 1, 0.01, 10^{-6}, 0.1)$. (*a*) Temporal variation of Σ_0 and $\langle H^2\rangle$ (dashed line), (*b*) h and ν (dashed line), and (*c*) q and ν (dashed line), all at $x=0$. (*d–f*) Time–space plots of membrane height, surface charge and trans-membrane potential from $T=59$ to $T=60$.

$T=42$ (thick solid curve). The insets show a zoomed region from $T=31$ (dashed curve) to $T=34$. In figure 9(*a*) we see that the membrane first makes a big step to the left from $T=31$ to $T=32$, then a small step to the right at $T=33$ and then again a big step to the left at $T=34$. Similar dynamics is found for q and V_m in figure 9(*b*) and figure 9(*c*), respectively. In figure 9(*d–f*) we show time–space plots sampled at multiples of the period. We clearly see a net movement from right to left in h in figure 9(*d*), q in figure 9(*e*) and V_m in figure 9(*f*). The membrane height can be quite close to the bottom electrode. Careful numerical convergence tests have been conducted to ensure that the nonlinear translational dynamics is not affected by h getting close to zero.

In deriving the long-wave equation the horizontal velocity on the membrane is set to zero for local membrane inextensibility at the leading order. Consequently the alternating wave is actually a 'coordinated' movement in the vertical direction like a Mexican wave in a soccer game: as the audience stands up and sits down in a rhythmic way, there appears to be a 'travelling wave' moving in a directed fashion. The nonlinear dynamics coordinates such individual movements into a travelling wave.

Increasing β further to $\beta=600$, we find that the unidirectional travelling wave is replaced by a sloshing wave moving back and forth, almost in synchrony with the AC field. However it is not clear how physically realizable it is to have $\beta=600$ in the microfluidic laboratory. We are now conducting a thorough numerical investigation of the parameter space $(\varepsilon_r, \sigma_r, \mu_r, g_m, \varkappa, \alpha)$ to check if there is other nonlinear dynamics that may be realizable in a microfluidic experiment.

4. Summary

In this work we investigated the long-wave nonlinear dynamics of an inextensible capacitive leaky (conducting) elastic membrane under electric fields. Using the sharp-interface approximation, the inextensible membrane behaves as a capacitive

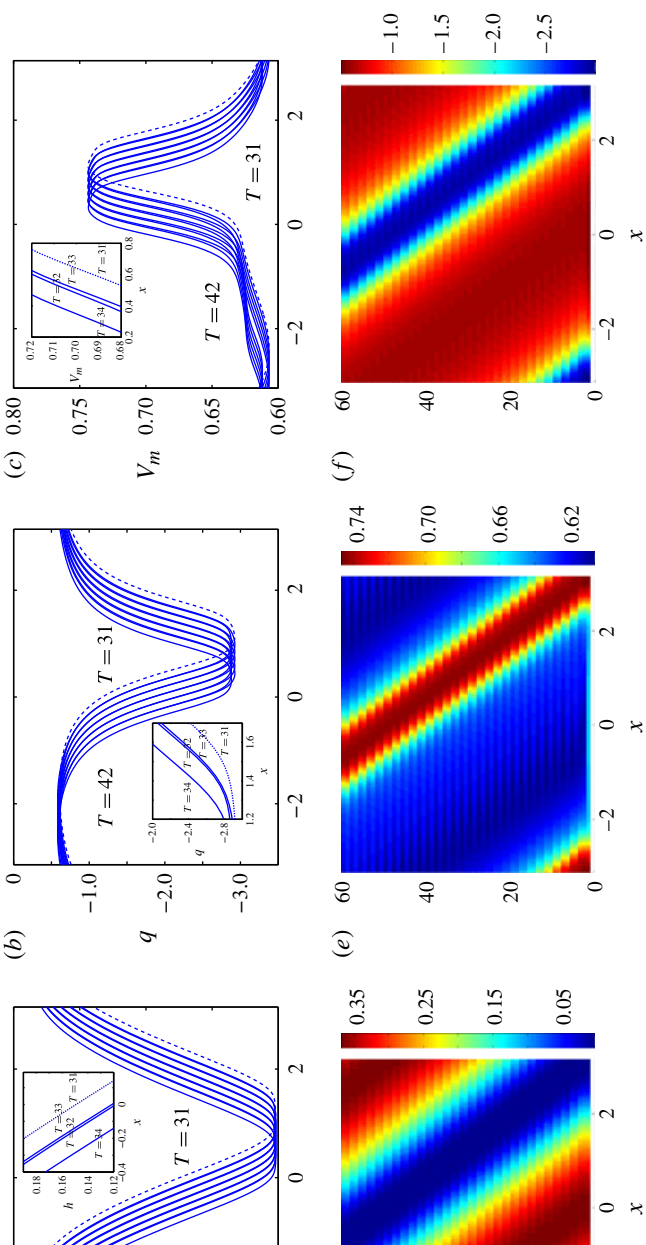

FIGURE 9. (Colour online) Temporal evolution at multiple periods of the AC field. (*a–c*) Evolution of the membrane height (*a*), surface charge (*b*) and trans-membrane potential (*c*) from $T = 31$ to $T = 42$. Insets show a zoomed region from $T = 31$ (dashed curve) to $T = 34$. (*d–f*). Space–time plots of h in (*d*), q in (*e*), and V_m in (*f*).

elastic sheet with a conductance due to ions leaking through the membrane. We derived a sixth-order nonlinear equation with an integral constraint from the membrane inextensibility in the long-wave limit. In a DC field where the displacement current is negligible, we analytically derived the equilibrium profile of a non-conducting membrane for a given excess length S and the area θ under the planar membrane. We implemented a semi-implicit iterative scheme to numerically investigate the nonlinear dynamics of the membrane. Our long-wave model captures the linear behaviour of a tensionless flat membrane, and we examined the different nonlinear dynamics under varying electric field strengths and excess length with physically relevant parameters in the simulations.

In our numerical simulations, both time step and grid spacing are adjusted to ensure that (i) the error in the excess length never exceeds 1 % of the initial excess length throughout the simulations, and (ii) numerically convergent solutions are obtained. Results in § 3.2 demonstrate the important role of membrane tension Σ_0 in membrane dynamics: periodic undulation and flip-flopping of a membrane are direct consequences of the linear instability of the membrane when the tension is close to zero. When the tension is significantly larger than zero, the membrane profile stays close to the equilibrium profile of a non-conducting membrane in a DC field. As summarized in § 2.2 these equilibrium profiles depend only on the excess length S and the area θ under the membrane. Results in § 3.3 show that the flip-flop of the membrane profile gives rise to overshoot in membrane height when the external electric potential ν is increasing, and the magnitude of overshoot increases with the excess length S. During the membrane flip-flop we also find the surface charge density focusing at $x = 0$ where the membrane height overshoots. Such charge focusing at the highest-curvature location of the membrane is reminiscent of Taylor cone formation in electrohydrodynamics (Fernandez de la Mora 2007).

Pillar formation from the instability of a fluid interface in an AC field has been observed using a lubrication model (Roberts & Kumar 2009, 2010). This pillar formation was not observed here for a membrane but we have observed a new type of nonlinear dynamics. In particular, at large excess length and under a strong AC field, we find that after two cycles of membrane flip-flop the membrane height can get very close to the bottom wall, where $\min(h) \approx 10^{-3}$ for results in figure 8(*d*), and then the membrane takes on a travelling motion with a double-periodic dynamics in the sequence: a big step to the right, a small step to the left and then a big step to the right. Careful numerical convergence tests have been conducted to ensure that sufficient numerical resolutions are used to guarantee numerically convergent results and that the travelling dynamics is not a numerical artifact. Within our long-wave formulation this dynamics can be described as a 'Mexican wave' for the 'coordinated' travelling wave moving in $2-1$ steps (two steps forward, one step back).

In electroformation where an AC field is used (Angelava & Dimitrov 1987; Constantin *et al.* 2005; Lecuyer *et al.* 2006; Le Berre *et al.* 2008), the AC field frequency is several Hz, the AC strength E_0 is often a few kilovolts per metre, $\sigma_1 \sim 10^{-4}$ S m^{-1}, the channel height is in the range $100\ \mu\text{m} \leqslant h_0 \leqslant 1$ mm and the channel aspect ratio usually satisfies $\epsilon \leqslant 0.3$ for a vesicle filling the channel ($\epsilon = 2r_0/2\pi r_0 = 1/\pi \sim 0.3$). In our non-dimensionalization, this gives a time scale $h_0 C_m/\sigma_1 \sim 10^{-1}\epsilon$ s. Thus the maximum growth rate from figure 3(*b*,*c*) (for a tensionless planar membrane in an AC field) gives an estimate of several seconds for significant membrane deformation due to linear instability, consistent with results in Seiwert & Vlahovska (2013). However, the membrane tension may soon become non-negligible as the membrane is under electric stress, and the linear results for a

tensionless membrane may not be relevant after a short time (a couple of minutes as opposed to close to an hour for vesicle formation in the experiments).

From our numerical simulations of an inextensible membrane under electric stress, we find that the electric field needs to be increased to several tens of kilovolts per metre for various nonlinear membrane dynamics. In practice the lipid bilayer membrane stays intact as the electric field strength goes up to $\sim$30 kV m^{-1} and the conductivity ratio can be as large as $\sim$40 (Sadik *et al.* 2011). Thus the parameters used in the simulations are physically realizable in the laboratory, even though no report of the three types of nonlinear membrane dynamics is found in the literature. In electroformation experiments a bilayer membrane can be initially stacked and in close contact with the substrate, hence it is possible that other factors (such as interaction with the substrate and electrolytes) or physics (finite thickness of the bilayer membrane) have to be included to explain the vesicle formation under an electric field. For a nearly perfect dielectric fluid (with vanishing electrical conductivity) the surface current is dominated by the displacement current. Therefore we expect that an extremely high electric field is needed to observe all three types of nonlinear membrane dynamics in a perfect dielectric fluid.

Our long-wave model can be modified to consider both (i) the van der Waals force between the membrane and electrodes, and (ii) the effect of disjoining pressure on the travelling wave and sloshing wave. In particular we are replacing the leaky dielectric fluids with electrolyte solutions where the bulk charges are not zero and the charges may accumulate away from the membrane. The membrane is found to be more linearly unstable in the presence of these charges near the membrane (Bazant *et al.* 2009). It will be interesting to revisit the nonlinear dynamics of the membrane in the electrolytic solution. In addition we are also incorporating the membrane asymmetry due to the mismatch in lipid composition between the two leaflets to examine how the asymmetry in the two leaflets might lead to different membrane dynamics and equilibrium shapes under external forces.

Acknowledgements

Y.-N.Y. acknowledges partial support from NSF grant DMS-1222550 and useful discussion with P. M. Vlahovska. S.V. acknowledges support from NSF grant DMS-1224656. M.J.M. acknowledges support from NSF grant DMS-1312935. The simulations were conducted on the NJIT computing cluster, supported by NSF/MRI grant number DMS-0420590.

Appendix A

The derivation of (2.10) for the transmembrane potential V_m can be found in Seiwert *et al.* (2012) and Seiwert & Vlahovska (2013). We reproduce those steps here for completeness (see also McConnell 2013).

Begin by considering the equations for the conservation of normal current density across the lipid monolayer facing side 1, located at $z = h_1(x, t)$ and facing side 2, located at $z = h_2(x, t)$. Note that we distinguish between each of these monolayers for the sake of this derivation but within our continuum model the bilayer lipid membrane interface has zero thickness and is located at $z = h(x, t)$. This results in the two conservation equations

$$\boldsymbol{n} \cdot (\boldsymbol{J}_1 - \boldsymbol{J}_m) = -\frac{\partial q_1}{\partial t} - \nabla_s \cdot (\boldsymbol{u} q_1) \quad \text{at } z = h_1, \tag{A 1}$$

$$\boldsymbol{n}\cdot(\boldsymbol{J}_m-\boldsymbol{J}_2)=-\frac{\partial q_2}{\partial t}-\nabla_s\cdot(\boldsymbol{u}q_2)\quad\text{at } z=h_2. \tag{A 2}$$

Here $\boldsymbol{J}_i=\sigma_i\boldsymbol{E}_i$ represents current density and q_i denotes the electric charge density along each side while $\boldsymbol{J}_m=\sigma_m\boldsymbol{E}_m$ is the ohmic current density crossing the membrane. This current leaking through the membrane $\boldsymbol{n}\cdot\boldsymbol{J}_m$ will be approximated by the voltage jump across the membrane times the membrane conductivity, i.e. $\boldsymbol{n}\cdot\boldsymbol{J}_m=G_mV_m$ The right-hand side of each of these equations represents the rate of change of charge along the monolayer of the moving interface. Using the incompressibility of the interface, $\nabla_s\cdot\boldsymbol{u}=0$, the convective term on the right-hand side of each equation can be replaced with $\boldsymbol{u}\cdot\nabla_s q_i$.

The surface charge density is given by $q_1=\boldsymbol{n}\cdot\varepsilon_1\boldsymbol{E}_1-\boldsymbol{n}\cdot\varepsilon_m\boldsymbol{E}_m=\boldsymbol{n}\cdot\varepsilon_1\boldsymbol{E}_1-C_mV_m$ at $z=h_1$, where the approximation $\boldsymbol{n}\cdot\varepsilon_m\boldsymbol{E}_m=C_mV_m$ is used for a thin membrane. Similarity along $z=h_2$ we have $q_2=C_mV_m-\boldsymbol{n}\cdot\varepsilon_2\boldsymbol{E}_2$. Note that this implies that the total charge is $q=q_1+q_2=\varepsilon_1E_1-\varepsilon_2E_2$ as given in § 2. Putting all of the above approximations into (A 1) and (A 2) then gives (2.10).

REFERENCES

ANGELOVA, M. I. & DIMITROV, D. S. 1986 Liposome electroformation. *Faraday Discuss. Chem. Soc.* **81**, 303–311.

ANGELAVA, M. I. & DIMITROV, D. S. 1987 Swelling of charged lipids and formation of liposomes on electrode surfaces. *Mol. Cryst. Liq. Cryst.* **152**, 89–104.

ANGELOVA, M. I., SOLEAU, S., MELEARD, PH., FAUCON, J. F. & BOTHEOREL, P. 1992 Preparation of giant vesicles by external ac electric fields. kinetics and applications. *Prog. Colloid Polym. Sci.* **89**, 127–131.

ANTOV, Y., BARBUL, A., MANTSUR, H. & KORENSTEIN, R. 2005 Electroendocytosis: exposure of cells to pulsed low electric fields enhances adsorption and uptake of macromolecules. *Biophys. J.* **88**, 2206–2223.

BAZANT, M. Z., KILIC, M. S., STOREY, B. D. & AJDARI, A. 2009 Towards an understanding of induced-charge electrokinetics at large applied voltages in concentrated solutions. *Adv. Colloid Interface Sci.* **152**, 48–88.

BEZLYEPKINA, R., DIMOVA, N., JORDO, M. D., KNORR, R. L., RISKE, K. A., STAYKOVA, M., VLAHOVSKA, P. M., YAMAMOTO, T., YANG, P. & LIPOWSKY, R. 2009 Vesicle in electric fields: some novel aspects of membrane behavior. *Soft Matt.* **5**, 3201–3212.

BLOUNT, M. J., MIKSIS, M. J. & DAVIS, S. H. 2012 Fluid flow beneath a semipermeable membrane during drying processes. *Phys. Rev.* E **85**, 016330.

CANUTO, C., HUSSAINI, M. Y., QUARTERONI, A. & ZANG, T. A. 1986 *Spectral Methods in Fluid Dynamics*. Springer.

CONSTANTIN, D., OLLINGER, C., VOGEL, M. & SALDITT, T. 2005 Electric field unbinding of solid-supported lipid multilayers. *Eur. Phys. J.* E **18**, 273–278.

CRASTER, R. V. & MATAR, O. K. 2005 Electrically induced pattern formation in thin leaky dielectric films. *Phys. Fluids* **17** (3), 032104.

FENG, J. Q. & BEARD, K. V. 1991 Three-dimenionsional oscillation characteristics of electrostatistically deformed drops. *J. Fluid Mech.* **227**, 429–447.

FERNANDEZ DE LA MORA, J. 2007 The fluid dynamics of Taylor cones. *Annu. Rev. Fluid Mech.* **39**, 217–243.

HOSOI, A. E. & MAHADEVAN, L. 2004 Peeling, healing, and bursting in a lubricated elastic sheet. *Phys. Rev. Lett.* **93**, 137802.

LACOSTE, D., LAGOMARSINO, M. C. & JOANNY, J. F. 2007 Fluctuations of a driven membrane in an electrolyte. *Europhys. Lett.* **77**, 18006.

LACOSTE, D., MENON, G. I., BAZANT, M. Z. & JOANNY, J. F. 2009 Electrostatic and electrokinetic contributions to the elastic moduli of a driven membrane. *Eur. Phys. J.* E **28**, 243–264.

LE BERRE, M., YAMADA, A., RECK, L., CHEN, Y. & BAIGL, D. 2008 Electroformation of giant phospholipid vesicles on a silicon substrate: advantages of controllable surface properties. *Langmuir* **24**, 2643–2649.

LECUYER, S., FRAGNETO, G. & CHARITAT, T. 2006 Effect of an electric field on a floating lipid bilayer: a neutron reflectivity study. *Eur. Phys. J.* E **21**, 153–159.

MALDARELLI, C. & JAIN, R. K. 1982 The linear, hydrodynamic stability of an interfacially perturbed, transversely isotropic, thin, planar viscoelastic film. *J. Colloid Interface Sci.* **90** (1), 233–262.

MALDARELLI, C., JAIN, R. K. & IVANOV, I. B. 1980 Stability of symmetric and unsymmetric thin liquid films to short and long wavelength perturbations. *J. Colloid Interface Sci.* **78** (1), 118–126.

MATLAB, 2012 *Version 8.0.0.783 (R2012b)*. The MathWorks, Inc.

MCCONNELL, L. C. 2013 A numerical investigation of the electrohydrodynamics of lipid bilayer vesicles. PhD thesis, Northwestern University, Evanston, IL.

MCCONNELL, L. C., MIKSIS, M. J. & VLAHOVSKA, P. M. 2013 Vesicle electrohydrodynamics in dc electric fields. *IMA J. Appl. Maths* **78**, 797–817.

ORON, A., DAVIS, S. H. & BANKOFF, S. G. 1997 Long-scale evolution of thin liquid films. *Rev. Mod. Phys.* **69**, 931–980.

PEASE, L. F. & RUSSEL, W. B. 2002 Linear stability analysis of thin leaky dielectric films subjected to electric fields. *J. Non-Newtonian Fluid Mech.* **102**, 233–250.

RISKE, K. A. & DIMOVA, R. 2005 Electro-deformation and poration of giant vesicles viewed with high temporal resolution. *Biophys. J.* **88**, 1143–1155.

ROBERTS, S. A. & KUMAR, S. 2009 AC electrohydrodynamic instabilities in thin liquid films. *J. Fluid Mech.* **631**, 255–279.

ROBERTS, S. A. & KUMAR, S. 2010 Electrohydrodynamic instabilities in thin liquid trilayer films. *Phys. Fluids* **22**, 122012.

SADIK, M. M., LI, J., SHAN, J. W., SHREIBER, D. I. & LIN, H. 2011 Vesicle deformation and poration under strong dc electric fields. *Phys. Rev.* E **83**, 066316.

SCHAFFER, E., THURN-ALBRECHT, T., RUSSELL, T. & STEINER, U. 2000 Electrically induced structure formation and pattern transfer. *Nature* **603**, 874–877.

SCHWALBE, J. T., VLAHOVSKA, P. M. & MIKSIS, M. 2011 Lipid membrane instability driven by capacitive charging. *Phys. Fluids* **23**, 04170.

SEIFERT, U. 1995 The concept of effective tension for fluctuating vesicles. *Z. Phys.* B **97**, 299–309.

SEIWERT, J., MIKSIS, M. J. & VLAHOVSKA, P. M. 2012 Stability of biomimetic membranes in DC electric fields. *J. Fluid Mech.* **706**, 58–70.

SEIWERT, J. & VLAHOVSKA, P. M. 2013 Instability of a fluctuating membrane driven by an ac electric field. *Phys. Rev.* E **87**, 022713.

SENS, P. & ISAMBERT, H. 2002 Undulation instability of lipid membranes under an electric field. *Phys. Rev. Lett.* **88**, 128102.

VAN SWAAY, D. & DEMELLO, A. 2013 Microfluidic methods for forming liposomes. *Lab on a Chip* **13**, 752–767.

THAOKAR, R. M. & KUMARAN, V. 2005 Electrohydrodynamic instability of the interface between two fluids confined in a channel. *Phys. Fluids* **17**, 084104.

TORNBERG, A.-K. & SHELLEY, M. J. 2004 Simulating the dynamics and interactions of flexible fibers in Stokes flows. *J. Comput. Phys.* **196**, 8–40.

VEERAPANENI, S. K., GUEFFIER, D., ZORIN, D. & BIROS, G. 2009 A boundary integral method for simulating the dynamics of inextensible vesicles suspended in a viscous fluid in 2d. *J. Comput. Phys.* **228** (7), 2334–2353.

WEAVER, J. C. & CHIZMADZHEV, Y. A. 1996 Theory of electroporation: a review. *Bioelectrochem. Bioenerg.* **41**, 135–160.

WU, N. & RUSSEL, W. B. 2009 Micro- and nano-patterns created via electrohydrodynamic instabilities. *Nanotoday* **4**, 180–192.

ZHANG, J., ZAHN, J. D., TAN, W. & LIN, H. 2013 A transient solution for vesicle electrodeformation and relaxation. *Phys. Fluids* **25**, 071903.

ZIEBERT, F., BAZANT, M. Z. & LACOSTE, D. 2010 Effective zero-thickness model for a conductive membrane driven by an electric field. *Phys. Rev.* E **81**, 031912.

ZIEBERT, F. & LACOSTE, D. 2010 A Poisson-Boltzmann approach for a lipid membrane in an electric field. *New J. Phys.* **12**, 095002.

ZIEBERT, F. & LACOSTE, D. 2011 A planar lipid bilayer in an electric field: membrane instability, flow field, and electrical impedance. *Adv. Planar Lipid Bilayers Liposomes* **14**, 63–95.